Letter

Predictability of isotropic turbulence by massive ensemble forecasting

Alberto Vela-Martín
Escuela Politécnica Superior, Universidad Carlos III de Madrid, 28911 Leganés, Spain

(Received 10 August 2023; accepted 17 September 2024; published 4 December 2024)

The predictability of isotropic turbulence is studied with unprecedented detail using massive Monte Carlo ensembles. Predictability loss is characterized by the smoothing of the ensemble-averaged flow field with the forecasting time, which is accurately captured by the ensembles. It is shown that this process is well described in scale and physical space by a Gaussian low-pass filter, with a characteristic length scale that increases in time following a self-similar scaling. These results simplify the quantification of uncertainty in turbulence forecasts and open the possibility to efficiently assess the predictability of local inertial- and large-scale flow patterns.

DOI: 10.1103/PhysRevFluids.9.L122601

Predicting natural phenomena is a fundamental goal of science with important practical implications. A relevant example is weather prediction, which is an essential activity with a strong social and economic impact [1]. The predictability of the atmosphere, in particular, and of turbulent flows, in general, is limited by model errors and, in a more fundamental way, by the amplification of the uncertainty in the initial conditions due to chaos [2–4]. A general estimate of predictability in chaotic systems is given by the Lyapunov exponents, which quantify the growth rate of infinitesimal perturbations [5–7]. In turbulence—a multiscale phenomenon—a more realistic measure of predictability is given by the nonlinear growth of finite-size perturbations across scales [8–11]. A practical problem not easily handled by measuring errors between pairs of trajectories is accurately quantifying the fluctuations of predictability in space and time. This is important in turbulent flows, in which relevant flow patterns are usually localized, for instance, extreme events [12–14] or coherent structures [15–17].

To characterize the local predictability of turbulent flows, it is convenient to address this problem in its most general sense—as described by a Liouville equation for the probability distribution of the possible states of the system [18]. Initially, this probability distribution is concentrated around the true state with a spread that represents our knowledge (or ignorance) of the initial conditions. At later times, the distribution extends across phase space due to chaos, increasing the number of different possible future states and reducing predictability. Directly integrating the Liouville equation is, in general, intractable due to the high dimensionality of turbulence, and even solving only for the first and second moments of the distribution represents a challenge due to closure problems [19].

A more practical approach is the ensemble forecasting method [20,21], in which sets of flow fields, or ensemble members, drawn from the initial probability distribution (which is usually unknown and needs to be modeled [22,23]) are integrated in time to estimate future probabilities. This approach allows a local characterization of predictability in terms of the local ensemble average and variance of the velocity field, but is limited by the high computational cost of producing large ensembles of well-resolved simulations, particularly to yield an accurate description of predictability [24].

In this Letter, massive Monte Carlo ensembles with thousands of direct numerical simulations are used to study the predictability of isotropic turbulence. This dataset captures accurately the smoothing of the ensemble-averaged flow with the lead time [20]. Since the ensemble-averaged flow constitutes the optimal least-square prediction, its smoothing represents the filtering out of unpredictable flow patterns. It is shown that this process can be well reproduced in scale and physical space by a low-pass Gaussian filter with a characteristic scale that increases with time. In the inertial range, this characteristic scale follows a Kolmogorov scaling, in agreement with the self-similar growth of finite-size perturbations [9,10,25]. It is shown that the ensemble-averaged flow largely reproduces the structure of the filtered true flow at the minimum predictable scale, particularly for the most intense events. These results suggest that predictability loss can be partly modeled in scale and physical space by a simple filtering operation, where the scale of the filter represents the minimum scale below which informative predictions of the velocity field are not possible.

Let us consider a homogeneous and isotropic turbulent flow contained in a triply periodic cubic box of volume $(2\pi)^3$. The evolution of the velocity field $\boldsymbol{u}(\boldsymbol{x}, t)$ is described by the incompressible Navier-Stokes equation (NSE)

$$\partial_t \boldsymbol{u} + \boldsymbol{u} \cdot \nabla \boldsymbol{u} = -\nabla p + \nu \nabla^2 \boldsymbol{u} + \boldsymbol{f}, \tag{1}$$

where p is the kinematic pressure, which enforces the incompressibility of the flow ($\nabla \cdot \boldsymbol{u} = 0$); ν is the kinematic viscosity; and $\boldsymbol{f}$ is a linear forcing that acts on the large scales to maintain a statistically steady state. These equations are projected on a Fourier basis with $N/2$ modes in each direction, where N is the number of grid points, and solved using standard pseudospectral methods (see Ref. [26] for details of the code and the forcing). The flow is characterized by the Reynolds number $\mathrm{Re}_\lambda = U\lambda/\nu$, where $\lambda = \sqrt{15(\nu/\varepsilon)}U$ is the Taylor microscale, ε is the average kinetic energy dissipation, and U is the root-mean-squared velocity fluctuations. The Kolmogorov length scale and timescale are $\eta = (\nu^3/\varepsilon)^{1/4}$ and $\tau = (\nu/\varepsilon)^{1/2}$, respectively, and the large-scale eddy-turnover time is $T = L/U$, where L is the integral scale of the longitudinal velocity autocorrelation [27]. Two Reynolds numbers are considered in this investigation, $\mathrm{Re}_\lambda = 195$ and 120, which are simulated on grids of $N = 256$ and 128 points, respectively. The resolution of the simulations is $k_{\max}\eta = 1$, where $k_{\max} = \sqrt{2}/3N$ is the largest resolved wave number. This resolution is smaller than in standard simulations [26], but this is justified by the very high computational cost of producing the ensembles, and in that the focus of this investigation is on scales above the dissipative range.

Predictability is studied here by Monte Carlo ensemble forecasting [20]. First, $\mathcal{N}_i = 10$ statistically independent initial conditions or base flows, $\boldsymbol{u}^i$, are selected from a very long simulation. The uncertainty of these initial conditions is modeled by adding small random perturbations to the base flows, $\boldsymbol{u}^{i,p} = \boldsymbol{u}^i + \delta\boldsymbol{\phi}$, where $\boldsymbol{\phi}$ is a random Gaussian vector field with zero mean and unit variance, δ controls the uncertainty, and $\boldsymbol{u}^i$ is the true state of the system in the sense that its evolution would be precisely recovered for all ensemble members for $\delta \to 0$. Perturbations are automatically projected by the code to satisfy continuity. The ensembles are initialized by producing $\mathcal{N}_p = 4000$ different perturbed initial conditions, $\boldsymbol{u}^{i,p}$, around each base flow with $\delta = 7 \times 10^{-3}U$. These perturbations are small compared to the velocity fluctuations at the Kolmogorov scale ($\delta < 10^{-2}\eta/\tau$), ensuring that they first evolve linearly and that they align with the most unstable modes of the flow before triggering nonlinear effects. Thus, the evolution of the perturbations becomes independent of the structure of the noise $\boldsymbol{\phi}$ in a short time.

The $\mathcal{N}_i$ ensembles of $\mathcal{N}_p$ perturbed flows are evolved for approximately $10T$, and the statistics of each ensemble (averages and variances) are stored approximately every $0.5T$. The number of ensemble members is enough to converge the ensemble average and variance of the velocity field with an uncertainty that is small in Kolmogorov units (see Supplemental Material [28]). The linear forcing induces large-scale fluctuations in timescales of the order of a few turnover times, leading to a nonequilibrium cascade [29]. These fluctuations are well represented by the collection of $\mathcal{N}_i$ base flows, which provide a statistically converged measure of predictability (see Supplemental Material [28]).

The predictability of each base flow $\boldsymbol{u}^i$ is analyzed through the ensemble-averaged flow field,

$$\{\boldsymbol{u}\}^i(\boldsymbol{x}, t) = \frac{1}{\mathcal{N}_p} \sum_p \boldsymbol{u}^{i,p}(\boldsymbol{x}, t), \tag{2}$$

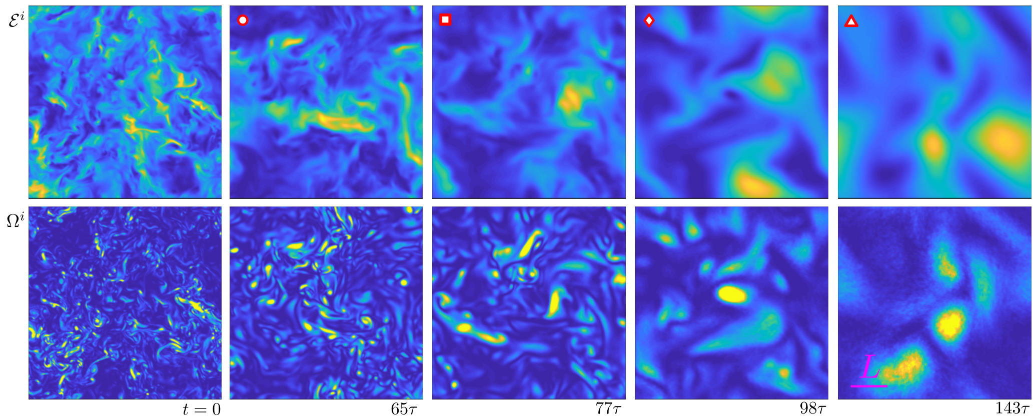

FIG. 1. Color plots of the kinetic energy, $\mathcal{E} = 1/2|\{\boldsymbol{u}\}^i|^2$ (top row), and the enstrophy, $\Omega = |\{\boldsymbol{\omega}\}^i|^2$ (bottom row), of the ensemble-averaged flow field as a function of time for $\mathrm{Re}_\lambda = 195$. The snapshots correspond, from left to right, to $t/\tau = 0$; 65, circle; 77, square; 98, diamond; and 143, triangle.

which is defined at each spatial coordinate $\boldsymbol{x}$ and evolves in time. This flow represents the optimal prediction of the future state of $\boldsymbol{u}^i$ in a least-square sense (it minimizes the mean-squared error with respect to all the members of the ensemble [20]), and its structure provides information on the features of the flow that are predictable. Figure 1 shows the evolution of cuts of the kinetic energy, $\mathcal{E}^i = 1/2|\{\boldsymbol{u}\}^i|^2$, and the enstrophy, $\Omega^i = |\{\boldsymbol{\omega}\}^i|^2$ ($\boldsymbol{\omega} = \nabla \times \boldsymbol{u}$ is the vorticity vector), of the ensemble-averaged flow field. Both $\mathcal{E}^i$ and Ω^i are progressively smoothed as time increases. In particular, the characteristic length scale of the vortical structures of Ω^i increases from η to L in approximately $80\tau \approx 4T$. This is a consequence of the short turnover time of the small scales, in which the ensemble members decorrelate fast, leading to the cancellation of the ensemble average [20].

Thus, the predictability loss is equivalent to a progressive filtering or damping of the small scales in the ensemble-averaged flow field. This process is characterized here using the instantaneous kinetic energy spectrum $E_{\{\boldsymbol{u}\}^i}(k,t) = 2\pi k^2 \langle \{\widehat{\boldsymbol{u}}\}^i \{\widehat{\boldsymbol{u}}^*\}^i \rangle_k$, where $\widehat{\boldsymbol{u}} = \mathcal{F}[\boldsymbol{u}]$ is the Fourier transform of the velocity field ($\mathcal{F}^{-1}$ is the inverse transform), the asterisk denotes the complex conjugate, $\boldsymbol{k}$ is the wave-number vector, $k = |\boldsymbol{k}|$ is its magnitude, and $\langle \cdot \rangle_k$ represents the average over spherical wave-number shells. Figure 2(a) shows the gradual loss of small-scale energy in the evolution of $E_{\{\boldsymbol{u}\}^i}$ in a single ensemble. This happens in parallel with an increment of the uncertainty, quantified by the spectral ensemble variance or spectral mean-squared error, $S^i(k,t) = \{E_{\boldsymbol{u}}\}^i - E_{\{\boldsymbol{u}\}^i}$, which grows in time from small to large scales, as shown in Fig. 2(b). Here S^i is equivalent to the average error spectrum between pairs of trajectories [4,8], but with errors measured with respect to the ensemble-averaged flow. The growth of S^i is proportional to the damping of the ensemble-averaged flow, which may be interpreted as a flux of energy from the predictable (correlated) to the unpredictable (uncorrelated) scales of the flow [30].

The separation between predictable and unpredictable scales is characterized by an exponential decay of $E_{\{\boldsymbol{u}\}^i}$. Consider the filtering operation $\widetilde{\boldsymbol{u}} = \mathcal{F}^{-1}[\widehat{\boldsymbol{u}} \cdot G(k,\ell)]$, where $G(k,\ell) = \exp(-k^2\ell^2/2\pi^2)$ is a Gaussian filter kernel. Taking the base flow $\boldsymbol{u}^i$ as a reference, let us find the filter scale $\ell^i(t)$ for which the total enstrophy of $\{\boldsymbol{u}\}^i$ is equal to that of the filtered base flow $\widetilde{\boldsymbol{u}}^i$, which is formulated in terms of the spectra as $\sum_k k^2 E_{\{\boldsymbol{u}\}^i} = \sum_k k^2 E_{\widetilde{\boldsymbol{u}}^i}$, where $E_{\widetilde{\boldsymbol{u}}^i} = E_{\boldsymbol{u}^i} G^2(k,\ell^i)$. As shown in Fig. 2(a), this condition provides a very good fit between $E_{\{\boldsymbol{u}\}^i}$ and $E_{\widetilde{\boldsymbol{u}}^i}$. This shows that predictability loss acts on the ensemble-averaged flow as a Gaussian low-pass filter, where $\ell^i(t)$ represents the minimum scale below which informative predictions of the velocity field are not possible.

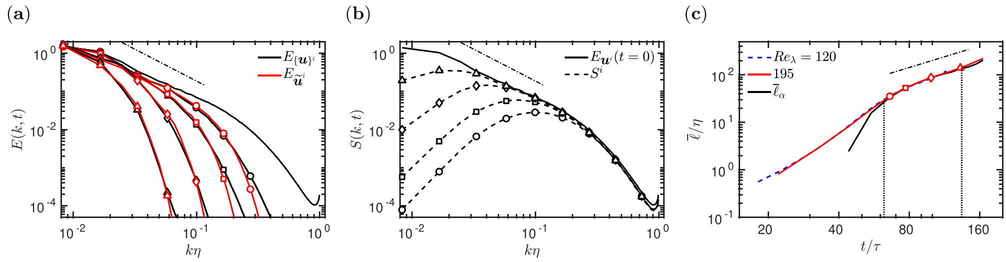

FIG. 2. (a) Instantaneous kinetic energy spectra of the ensemble-averaged field $E_{\{\boldsymbol{u}\}^i}$, and the filtered base flow $E_{\widetilde{\boldsymbol{u}}^i}$ at scale ℓ^i. (b) Instantaneous spectral variance $S^i(k,t)$. The data in (a) and (b) correspond to the same ensemble ($\mathrm{Re}_\lambda = 195$) and times as in Fig. 1. The solid lines without markers correspond to $t = 0$, and the lines with markers correspond to $t/\tau = 65$ (circle), 77 (square), 98 (diamond), and 143 (triangle). The dashed-dotted line marks $E \sim k^{-5/3}$. (c) Temporal evolution of the average minimum predictable scale $\overline{\ell}$; solid line, $\mathrm{Re}_\lambda = 195$; dashed line, $\mathrm{Re}_\lambda = 120$ (shifted to the temporal origin by $5.8T$); and black line, $\overline{\ell_\alpha}$ scaled by a factor of 1.7. The vertical lines mark between 30η and $L = 144\eta$. The dashed-dotted lines are proportional to $\ell \sim t^{3/2}$. Markers are as in Fig. 1.

The temporal evolution of $\ell^i(t)$ averaged over the $\mathcal{N}_i$ ensembles, $\overline{\ell}(t) = \mathcal{N}_i^{-1}\sum_i \ell^i(t)$, is shown in Fig. 2(c). The standard deviation of $\ell^i(t)$ across ensembles is small, $(\overline{\ell^2} - \overline{\ell}^2)^{1/2} \approx 0.05\overline{\ell}$, so that the evolution of $\overline{\ell}(t)$ is representative of the individual ensembles. For inertial scales ($65\tau < t < 150\tau$ and $30\eta < \overline{\ell} < 144\eta$ at $\mathrm{Re}_\lambda = 195$), $\overline{\ell}$ seems to approach a power-law regime consistent with Kolmogorov's scaling, $\overline{\ell} \sim t^{3/2}$. This incipient scaling is in agreement with the self-similar growth of errors reported in models [9,25,30] and direct numerical simulations [10] of isotropic turbulence at high Reynolds numbers. In fact, ℓ^i is proportional to the characteristic scale of the flow with a prescribed error-to-energy ratio, as defined in Refs. [10,30]. This scale is redefined here as $\ell_\alpha = \pi/k_\alpha$, where k_α fulfills $S^i(k_\alpha,t) = \alpha\{E_{\boldsymbol{u}}\}^i(k_\alpha,t)$ and α is a threshold. As shown in Fig. 2(b), for $\alpha = 0.95$, ℓ_α is proportional to ℓ^i in the inertial range. In addition, there is a very good collapse between $\overline{\ell}$ for $\mathrm{Re}_\lambda = 195$ and $\mathrm{Re}_\lambda = 120$, but the latter needs to be time-shifted towards the past due to the different magnitude of the initial perturbation and of the leading Lyapunov exponents in Kolmogorov units [5,6,10].

Let us now focus on the relation between the ensemble-averaged flow, $\{\boldsymbol{u}\}^i$, and the filtered true trajectory, $\widetilde{\boldsymbol{u}}^i$, in physical space, which is analyzed using the correlation coefficient $\rho(\boldsymbol{\phi},\boldsymbol{\psi}) = \langle\boldsymbol{\phi}\cdot\boldsymbol{\psi}\rangle/[s(\boldsymbol{\phi})s(\boldsymbol{\psi})]$, where $s(\boldsymbol{\phi}) = \langle|\boldsymbol{\phi}|^2\rangle$, and the brackets mark the space average. Figure 3(a) displays the correlation coefficient $\rho(\{\boldsymbol{u}\}^i,\widetilde{\boldsymbol{u}}^i)$ averaged over all the ensembles $\overline{\rho}$ as a function of $\overline{\ell}(t)$; in the inertial range, $\overline{\rho} > 0.9$. To better represent the structures at inertial scales, the correlation is computed for the vorticity vector $\rho(\{\boldsymbol{\omega}\}^i,\widetilde{\boldsymbol{\omega}}^i)$. In this case, $\overline{\rho}$ decreases for $\overline{\ell}$ in the viscous range but reaches a plateau with $\overline{\rho} \approx 0.8$ in the inertial range. This suggests that the high correlation should persist in a wider inertial range and is not a low-Reynolds-number effect. Interestingly, the correlation increases to approximately 0.9 when the spatial averages in the computation of ρ are restricted to the 10% most intense events of $\Omega^i = |\{\boldsymbol{\omega}\}^i|^2$ in each flow field, as shown also in Fig. 3(a). Visual evidence of this strong correlation is presented in Fig. 3(b), in which contours of high enstrophy of the filtered true flow, $\widetilde{\Omega}^i = |\widetilde{\boldsymbol{\omega}}^i|^2$, are plotted against the enstrophy of the ensemble-averaged flow. There is a good collapse of the intense structures, corroborating that they are particularly well captured by the ensemble-averaged flow field. Since this field represents the optimal least-square prediction, this suggests that intense structures appear to be more predictable than the weak turbulent background. This could be a consequence of their intensity, which would provide a shield from background perturbations and allow them to remain coherent for long times [17], or of a strong coupling to large scales [31,32]; further research is necessary to elucidate this question.

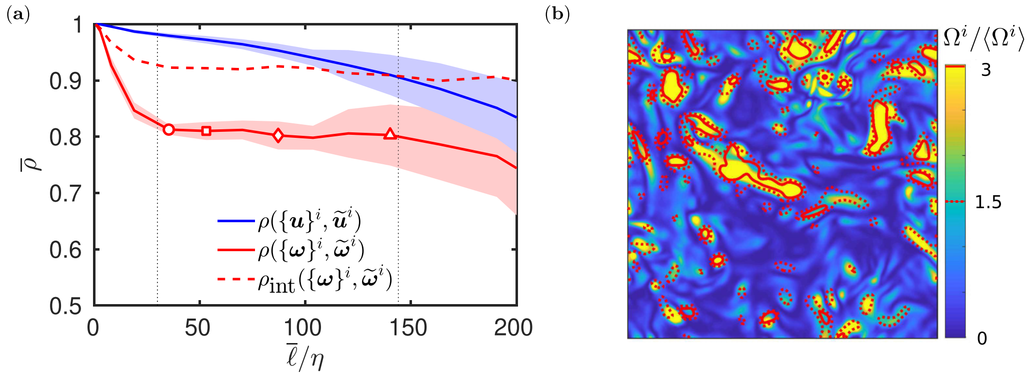

FIG. 3. (a) Correlation coefficient averaged over all the base flows as a function of $\overline{\ell}$; ρ_{int} corresponds to the correlation conditioned to intense enstrophy events, and the horizontal dotted lines mark the inertial range $30\eta < \overline{\ell} < L$. The markers correspond to the same times as the snapshots of Fig. 1, and the shaded areas correspond to± the standard deviation of the correlation across ensembles. (b) Comparison between the enstrophy of the enseble-averaged flow, Ω^i (colormap), and the enstrophy of the filtered true flow, $\widetilde{\Omega}^i$ [red contours at two intensities: $\widetilde{\Omega}^i/\langle\widetilde{\Omega}^i\rangle = 1.5$ (dotted line) and 3 (solid line)], for $t/\tau = 66$ and $\ell^i = 40\eta$. Data at $\text{Re}_\lambda = 195$.

In conclusion, the loss of predictability in isotropic turbulence can be represented in scale and physical space by a time-dependent Gaussian filter, which removes the unpredictable features of the flow. The filter scale increases in time according to an inertial scaling which depends only on the dissipation (or the inertial energy flux) and the forecasting time. These results show that filtering at suitably defined scales could be used to construct efficient estimators of the ensemble average, which would allow one to study the predictability of local flow features, e.g., extreme events or coherent structures, with small ensembles.

The similarities between ensemble averaging and Gaussian filtering revealed here suggest that uncertainty growth in turbulence forecasts could be modeled following large eddy simulation (LES) techniques. In fact, applying the ensemble-averaged operator to the NSE yields an equation similar to that of LES:

$$\partial_t\{\boldsymbol{u}\} + \{\boldsymbol{u}\}\cdot\nabla\{\boldsymbol{u}\} = -\nabla\{p\} + \nu\nabla^2\{\boldsymbol{u}\} + \{\boldsymbol{f}\} + \nabla\cdot\boldsymbol{\tau}^\dagger, \tag{3}$$

where the tensor $\boldsymbol{\tau}^\dagger = \{\boldsymbol{u}\}\{\boldsymbol{u}\}^{\mathrm{T}} - \{\boldsymbol{u}\boldsymbol{u}^{\mathrm{T}}\}$ (the superscript T denotes the transpose) represents the effect of the unpredictable scales on the predictable ones and is equivalent to the subgrid-scale stress tensor in LES [33]. Contracting Eq. (3) with $\{\boldsymbol{u}\}$ leads to an equation for the energy of the ensemble-averaged flow in which a term analogous to the subgrid scale energy transfer [34], $\Pi^\dagger = -\{\nabla\boldsymbol{u}\} : \boldsymbol{\tau}^\dagger$, represents a local conservative flux of energy from the ensemble average to the ensemble variance (see the Supplemental Material [28] for the full equations). The extensive research on interscale energy transfer in turbulence [35–39] could be leveraged to characterize predictability loss in terms of a space-local error "cascade" described by $\Pi^\dagger$. This is a promising research direction with potential applications to atmospheric flows (e.g., two-dimensional turbulence [40]), ensemble forecast initiation [22], data assimilation techniques [31,41,42], and uncertainty quantification [43].

[1] Y. Zhu, Z. Toth, R. Wobus, D. Richardson, and K. Mylne, The economic value of ensemble-based weather forecasts, Bull. Am. Meteorol. Soc. **83**, 73 (2002).

[2] E. Lorenz, A study of the predictability of a 28-variable atmospheric model, Tellus **17**, 321 (1965).

[3] E. Lorenz, The predictability of a flow which possesses many scales of motion, Tellus **21**, 289 (1969).
[4] G. Boffetta, M. Cencini, M. Falcioni, and A. Vulpiani, Predictability: a way to characterize complexity, Phys. Rep. **356**, 367 (2002).
[5] P. Mohan, N. Fitzsimmons, and R. D. Moser, Scaling of Lyapunov exponents in homogeneous isotropic turbulence, Phys. Rev. Fluids **2**, 114606 (2017).
[6] A. Berera and R. D. J. G. Ho, Chaotic properties of a turbulent isotropic fluid, Phys. Rev. Lett. **120**, 024101 (2018).
[7] A. Berera and D. Clark, Information production in homogeneous isotropic turbulence, Phys. Rev. E **100**, 041101(R) (2019).
[8] E. Aurell, G. Boffetta, A. Crisanti, G. Paladin, and A. Vulpiani, Predictability in systems with many characteristic times: The case of turbulence, Phys. Rev. E **53**, 2337 (1996).
[9] E. Aurell, G. Boffetta, A. Crisanti, G. Paladin, and A. Vulpiani, Predictability in the large: an extension of the concept of Lyapunov exponent, J. Phys. A **30**, 1 (1997).
[10] G. Boffetta and S. Musacchio, Chaos and predictability of homogeneous-isotropic turbulence, Phys. Rev. Lett. **119**, 054102 (2017).
[11] J. Ge, J. Rolland, and J. Vassilicos, The production of uncertainty in three-dimensional Navier–Stokes turbulence, J. Fluid Mech. **977**, A17 (2023).
[12] L. Biferale, F. Bonaccorso, I. M. Mazzitelli, M. A. T. van Hinsberg, A. S. Lanotte, S. Musacchio, P. Perlekar, and F. Toschi, Coherent structures and extreme events in rotating multiphase turbulent flows, Phys. Rev. X **6**, 041036 (2016).
[13] M. Farazmand and T. Sapsis, A variational approach to probing extreme events in turbulent dynamical systems, Sci. Adv. **3**, e1701533 (2017).
[14] D. Buaria, A. Pumir, E. Bodenschatz, and P.-K. Yeung, Extreme velocity gradients in turbulent flows, New J. Phys. **21**, 043004 (2019).
[15] G. Haller and G. Yuan, Lagrangian coherent structures and mixing in two-dimensional turbulence, Phys. D (Amsterdam, Neth.) **147**, 352 (2000).
[16] M. Green, C. Rowley, and G. Haller, Detection of lagrangian coherent structures in three-dimensional turbulence, J. Fluid Mech. **572**, 111 (2007).
[17] J. Jiménez, Coherent structures in wall-bounded turbulence, J. Fluid Mech. **842**, P1 (2018).
[18] T. Palmer, Predicting uncertainty in forecasts of weather and climate, Rep. Prog. Phys. **63**, 71 (2000).
[19] E. S. Epstein, Stochastic dynamic prediction, Tellus **21**, 739 (1969).
[20] C. Leith, Theoretical skill of Monte Carlo forecasts, Mon. Weather Rev. **102**, 409 (1974).
[21] M. Leutbecher and T. Palmer, Ensemble forecasting, J. Comput. Phys. **227**, 3515 (2008).
[22] Z. Toth and E. Kalnay, Ensemble forecasting at NCEP and the breeding method, Mon. Weather Rev. **125**, 3297 (1997).
[23] R. Buizza and T. Palmer, The singular-vector structure of the atmospheric global circulation, J. Atmos. Sci. **52**, 1434 (1995).
[24] M. Leutbecher, Ensemble size: How suboptimal is less than infinity? Q. J. R. Meteorol. Soc. **145**, 107 (2019).
[25] C. Leith and R. Kraichnan, Predictability of turbulent flows, J. Atmos. Sci. **29**, 1041 (1972).
[26] J. Cardesa, A. Vela-Martín, and J. Jiménez, The turbulent cascade in five dimensions, Science **357**, 782 (2017).
[27] S. Pope, *Turbulent Flows* (Cambridge University, Cambridge, England, 2001).
[28] See Supplemental Material at http://link.aps.org/supplemental/10.1103/PhysRevFluids.9.L122601 for the temporal statistics of the base flows, an analysis on the uncertainty in the estimation of the ensemble averaged flow and variance, and the equations describing the evolution of the ensemble average and variance.
[29] S. Goto and J. C. Vassilicos, Unsteady turbulence cascades, Phys. Rev. E **94**, 053108 (2016).
[30] O. Métais and M. Lesieur, Statistical predictability of decaying turbulence, J. Atmos. Sci. **43**, 857 (1986).
[31] A. Vela-Martín, The synchronisation of intense vorticity in isotropic turbulence, J. Fluid Mech. **913**, R8 (2021).

[32] C. C. Lalescu and M. Wilczek, Transitions of turbulent superstructures in generalized Kolmogorov flow, Phys. Rev. Res. **3**, L022010 (2021).

[33] C. Meneveau and J. Katz, Scale-invariance and turbulence models for large-eddy simulation, Annu. Rev. Fluid Mech. **32**, 1 (2000).

[34] G. Eyink and H. Aluie, Localness of energy cascade in hydrodynamic turbulence. I. Smooth coarse graining, Phys. Fluids **21**, 115107 (2009).

[35] V. Borue and S. A. Orszag, Local energy flux and subgrid-scale statistics in three-dimensional turbulence, J. Fluid Mech. **366**, 1 (1998).

[36] J. Cardesa, A. Vela-Martín, S. Dong, and J. Jiménez, The temporal evolution of the energy flux across scales in homogeneous turbulence, Phys. Fluids **27**, 111702 (2015).

[37] M. Buzzicotti, M. Linkmann, H. Aluie, L. Biferale, J. Brasseur, and C. Meneveau, Effect of filter type on the statistics of energy transfer between resolved and subfilter scales from a-priori analysis of direct numerical simulations of isotropic turbulence, J. Turbul. **19**, 167 (2018).

[38] P. L. Johnson, Energy transfer from large to small scales in turbulence by multiscale nonlinear strain and vorticity interactions, Phys. Rev. Lett. **124**, 104501 (2020).

[39] P. L. Johnson, A physics-inspired alternative to spatial filtering for large-eddy simulations of turbulent flows, J. Fluid Mech. **934**, A30 (2022).

[40] G. Boffetta and R. Ecke, Two-dimensional turbulence, Annu. Rev. Fluid Mech. **44**, 427 (2012).

[41] P. C. Di Leoni, A. Mazzino, and L. Biferale, Synchronization to big data: Nudging the Navier-Stokes equations for data assimilation of turbulent flows, Phys. Rev. X **10**, 011023 (2020).

[42] V. Mons, Y. Du, and T. A. Zaki, Ensemble-variational assimilation of statistical data in large-eddy simulation, Phys. Rev. Fluids **6**, 104607 (2021).

[43] K. Duraisamy, G. Iaccarino, and H. Xiao, Turbulence modeling in the age of data, Annu. Rev. Fluid Mech. **51**, 357 (2019).